



Cite this: *RSC Adv.*, 2024, 14, 15281

Hydrothermal synthesis of Mg/Al-layered double hydroxide modified water hyacinth hydrochar for remediation of wastewater containing mordant brown dye†

Saadia M. Waly,^a Ahmad M. El-Wakil,^a Weam M. Abou El-Maaty^a
and Fathi S. Awad *^{ab}

A high-performance dye adsorbent of Mg/Al-layered double hydroxide modified water hyacinth hydrochar (MgAl@WH) was synthesized by a simple hydrothermal method. The surface functional groups, elemental composition, crystalline structure, and surface morphology of the prepared (MgAl@WH) were determined using different analytical techniques. The characterization results revealed that the (MgAl@WH) hydrochar surface offered more active adsorption sites, facilitating the mordant brown (anionic dye) adsorption, leading to its superior performance with much higher uptake capability (311.0 mg g⁻¹ at 298 K) than Mg/Al double hydroxide nanosheets (MgAl DLHs, 80.2 mg g⁻¹ at 298 K) and dried water hyacinth (WH, 10.0 mg g⁻¹ at 298 K). The adsorption behavior of MgAl@WH follows the pseudo second order kinetic model ($R^2 = 0.999$) and Langmuir isotherm model ($R^2 = 0.999$). Moreover, MgAl@WH bonded efficiently with mordant brown dye via hydrogen bonding and interlayer anion exchange with monolayer formation. Additionally, the recycling tests revealed that the MgAl@WH can be reused over 10 cycles without significant change in the removal efficiency. Based on the obtained findings, Mg/Al-layered double hydroxide modified water hyacinth hydrochar (MgAl@WH), for its economic and environmental benefits, has recently been used as an efficient adsorbent to remediate industrial wastewater containing anionic dyes.

Received 8th April 2024

Accepted 6th May 2024

DOI: 10.1039/d4ra02624a

rsc.li/rsc-advances

1. Introduction

Water pollution by synthetic organic dyes has attracted a lot of public attention due to their high toxicity, resistance to degradation, easy accumulation in living things, and carcinogenicity. Up to 15–20% of the dyes used in textile dyeing processes are lost in wastewater because they do not attach to the fibers.^{1–3} Because of the complexity of wastewater, and, in particular, the existence of the hazardous azo-reactive dyes (mordant brown 15 (anionic dye)), color removal is considered one of the biggest concerns for the textile sector. Several Middle East regions have implemented stringent environmental regulations concerning

the colour restrictions of industrial effluent discharge; hence, the development of an efficient method for removing colour has become imperative.^{2–5} Several chemical,⁶ physical, and biological strategies⁷ have been investigated to take the colour out of industrial effluents with the aim of minimizing their environmental impact. These include adsorption,⁴ distillation,⁸ membrane separation,⁹ ultra-filtration,¹⁰ chemical oxidation,⁶ ozonation,¹¹ flocculation,¹⁰ photo catalytic degradation,¹² and chemical precipitation.¹⁰ Among them, the adsorption process is regarded as an inexpensive and effective process for the decontamination of the effluents of textile industries. Carbon-based materials (carbon nanotubes,¹³ graphene oxide,¹⁴ and activated carbon¹⁵) and synthetic resins¹⁶ are commonly employed in sorption processes to achieve high removal efficiency. However, remediation of water using these adsorbents is expensive because of their high production costs. There is still a need for the development of alternative sorbents, especially for low cost sorbents.

Biochar is defined as pyrogenic carbonaceous residues that are obtained by the thermochemical breakdown of biomass in an environment with limited oxygen or anoxia.^{17,18} According to recent studies, biochar is considered one of the most promising, cutting-edge, and affordable adsorbents for wastewater

^aChemistry Department, Faculty of Science, Mansoura University, Mansoura 35516, Egypt. E-mail: fathyawad949@yahoo.com; Tel: +201000166374

^bChemistry Department, Faculty of Science, New Mansoura University, New Mansoura, 35712, Egypt

† Electronic supplementary information (ESI) available: Instruments (S1); remediation of various anionic dyes using MgAl LDHs and/or biochars prepared through different reported methods (Table S1). Determination of pH_{PZC} (S2). The Freundlich and Langmuir and isotherm models eqn (S3). The PSO and PFO kinetic model equations (S4). Impact of temperature on mordant brown dye adsorption onto MgAl@WH biochar (Fig. S1). FTIR spectra of MgAl@WH biochar after 10 cycles (Fig. S2). See DOI: <https://doi.org/10.1039/d4ra02624a>

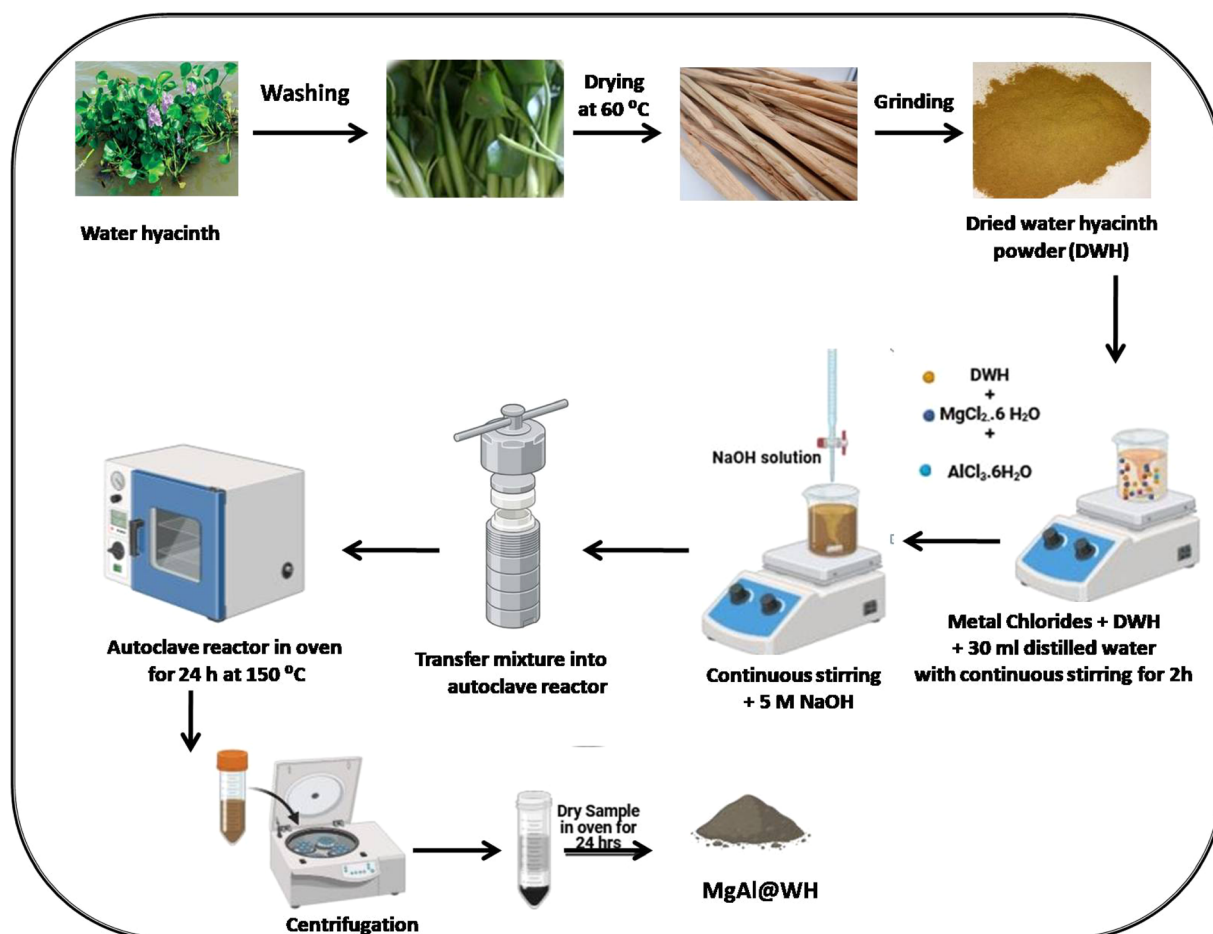


treatment.^{17–20} It is theoretically possible to produce biochar by hydropyrolysis, vacuum pyrolysis, slow pyrolysis or fast pyrolysis from any carbon-rich material, such as plant residues, agricultural wastes, animal litters, and solid wastes.^{17,19} The hydrothermal carbonization method (HTC) has recently a great attention because it is thought to be a very practical, simple, low-energy consumption, and straightforward way to transform different kinds of natural raw biomass into biochar.^{21–24} HTC is often carried out by mimicking the natural coalification process using subcritical water as the reaction medium at saturated pressure and mild temperatures between 160 and 300 °C. Comparing to other pyrolysis methods, the hydrothermal carbonization method is a gentler and more environmentally friendly method of producing biochars by reducing greenhouse gas emissions and tar production. Additionally, biochars with higher oxygen content, such as lactonic, phenolic, and carboxylic groups, can be produced using the HTC method.^{21–24}

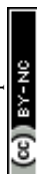
Water hyacinth (WH) is globally recognized as one of the most productive plants on the earth and is classified as the one of 100 most aggressive alien species in the natural world. The aquatic ecosystems and their biodiversity are negatively impacted by the excessive growth of water hyacinth.^{25,26} Typically, water hyacinth is mechanically gathered and then haphazardly scattered throughout the land without a practical

way to get rid of it. Water hyacinth composes of cellulose, hemicellulose, and lignin which can be easily converted into biochar through pyrolysis.^{25–27} Consequently, the production of biochar from water hyacinth offers the benefits of a large raw material supply, low cost, and excellent adsorption performance.^{26,27} The water hyacinth biochar has gained increasing attention as a potential material for wastewater treatment due to its has treatment distinctive properties (*i.e.*, high porosity, high surface area and abundant functional groups). However, the negatively charged surface of the prepared biochar has a low tendency toward the uptake of anionic organic contaminants owing to electrostatic repulsions. Consequently, the production of chemically modified biochar by intercalation metal cations (*i.e.*, Ca, Al, Mg, Fe) onto biochar matrix may enhance anionic dyes adsorption.²⁰ For example, biochar modified with AlOOH ,²⁸ Mg doped sugarcane straw biochar,²⁹ biochar-CuFe-CNC bio-composites²⁶ and magnetic biochar. Layered double hydroxides, LDHs, have drawn a lot of attention lately for their potential uses in water remediation.⁵ High surface area, easy synthesis, and superior ion exchange capacities are the main characteristics of LDHs that make them good choices for water treatment.^{5,20}

Mg/Al-layered double hydroxide modified water hyacinth biochar has never been utilized to remediate water containing



Scheme 1 The general procedure for the preparation of MgAl@WH biochar.



mordant brown 15 (anionic dye) in the literature. Therefore, this manuscript described the synthesis of the novel adsorbent Mg/Al LDHs-biochar (MgAl@WH) and its application for the removal of mordant brown dye from industrial effluents. Mg/Al LDHs-biochar composite was engineered for the first time from dried water hyacinth through a simple hydrothermal carbonization method. Mg/Al LDHs-biochar composite is a novel adsorbent owing to its unique chemical structure and easy synthetic strategy. The production of the biochar and the formation of the MgAl LDHs were done in one hydrothermal step to generate a nanocomposite with unique physicochemical properties. It is being predicted that the composite has high surface area that originated from the highly porous biochar derived from water hyacinth and homogenous distribution of MgAl LDHs which act as active sites for the adsorption of anionic dye from industrial effluents. The morphology and the chemical structure of the modified biochar were characterized using various analytical methods including TEM, SEM, XRD, XPS and FTIR. The Mg/Al-layered double hydroxide modified water hyacinth biochar (MgAl@WH) was used as superior adsorbent for the removal of mordant brown dye from aqueous solution. We also studied the influence of various parameters such as pH, initial dye concentration, time, temperature, recovery and recycling. In addition, MgAl@WH was utilized for the organic dyes removal from real water samples. The general procedure for the synthesis of MgAl@WH is shown in Scheme 1.

2. Materials and methods

2.1. Materials

High-purity chemicals purchased from Sigma-Aldrich were employed throughout the investigation without further purification including: $\text{AlCl}_3 \cdot 6\text{H}_2\text{O}$ (99.0%), $\text{MgCl}_2 \cdot 6\text{H}_2\text{O}$ (99.0%), NaOH (99.0%), EDTA (99.0%). Mordant brown 15 dye (Mordant brown) was purchased from the Dye Star Company, Brazil. Distilled water was utilized throughout the process. Water hyacinth (WH) used in this work was harvested in July, 2023, from river Nile in Dekerns city, Egypt. For more details on instruments, see ESI S1.†

2.2. Preparation of Mg/Al-layered double hydroxide modified water hyacinth biochar

Water hyacinth (WH) used in this work was harvested in July, 2023, from river Nile in Dekerns city, Egypt. Water hyacinth stems separated from the plant were rinsed with tap water 3–5 times to get rid of any unwanted material, such as dirt, grass, mud, and other plant species that were stuck on them, followed by washing with distilled water, and then dried at 60 °C for three to five days until their weight remained constant. To remove any metals adsorbed on the plant tissues, the dried water hyacinth stems were soaked in 0.25 M EDTA at pH 10 for 24 hours. They were then rinsed with distilled water until a pH of 6–8 was obtained and finally dried in oven at 80 °C for 2–3 days. Subsequently, the dried biomass was ground to pass through a 1 mm sieve was used for hydrothermal biochar production. The MgAl@WH biochar was prepared by dispersing 0.5 g of water

hyacinth powder in 30 mL distilled water by sonication for 15 min. After that, 1.0165 g of $\text{MgCl}_2 \cdot 6\text{H}_2\text{O}$ and 0.6035 g of $\text{AlCl}_3 \cdot 6\text{H}_2\text{O}$ were added to the WH suspension and stirred for 2 h at room temperature. Then, the pH of the solution was adjusted to 10 by stepwise adding sodium hydroxide (5.0 mol L^{-1}) with continuous stirring for 30 minutes. Subsequently, the mixture was transferred into a 100 mL Teflon container, sealed within a stainless steel reactor, and heated to 150 °C for a day. The product (MgAl@WH) was eventually allowed to cool to room temperature, centrifuged, rinsed with distilled water, ethanol, and dried overnight at 80 °C. For comparison, magnesium/aluminum layered double hydroxide nanosheets (MgAl DLH) was also prepared using the same procedure.

2.3. Dye adsorption studies

The adsorption of mordant brown (anionic dye) dye from aqueous solution using MgAl DLH, WH and MgAl@WH were carried out in 100 mL glass tubes containing 50 mL of mordant brown dye solution and 0.05 g of the adsorbent at appropriate conditions (pH and initial day concentration) followed by stirring for 2 h at 250 rpm. The influence of solution pH was conducted within the pH range (2–10) at 100 mg L^{-1} initial dye concentration. The desired initial pH was obtained using sodium hydroxide (0.01 M) or hydrochloric acid (0.01 M). Adsorption isotherm was performed by mixing 0.05 g of MgAl@WH biochar with 50 mL of mordant brown dye within the initial dye concentration range (1.0–600.0 ppm) at 5.5 (pH), 25 °C (temperature) and 2 h (agitation time). Additionally, the impact of temperature was also investigated according to the trials under 25 °C, 40 °C, and 50 °C, respectively. All the suspensions were separated by centrifugation and the supernatant dye concentrations were determined spectrophotometry at maximum absorption wavelength (530 nm). The impact of agitation time was conducted at 500 ppm initial dye concentration by collecting solution samples at various time intervals (5–240 min). In order to evaluate the impact of adsorbent dosage on mordant brown dye adsorption, different dosages (0.5–3 g L^{-1}) of MgAl@WH biochar were mixed with 50 mL of mordant brown dye solution (500 mg L^{-1}). The calculations of the adsorption capacity (q_e) in mg g^{-1} and adsorption efficiency (% E) were done using eqn (1) and (2), respectively.³⁰

$$q_e = \frac{(C_0 - C_e)V}{m} \quad (1)$$

$$\% E = \frac{(C_0 - C_e)}{C_0} \times 100 \quad (2)$$

where m (g) is the MgAl@WH biochar weight; V (L) is the solution volume; C_e and C_0 (mg g^{-1}) are the equilibrium and initial concentrations of mordant brown dye, respectively.

2.3.1. Reusability study. Desorption experiments were performed in order to evaluate the adsorbents' capability for reuse. After each adsorption cycle, 40 mg of the dye – loaded biochar was added to 100 mL glass vial containing 40 mL of 0.01 M NaOH and stirred for 2 h at 25 °C to ensure complete desorption. The suspension was then separated by



centrifugation. After washing several times with distilled water, the regenerating adsorbent was dried in oven at 80 °C and employed for further adsorption trials.

2.3.2. Real water samples. The adsorption of mordant brown dye (50 ppm) from a variety of real water samples, including household wastewater, Nile River water, tap water, and groundwater, was done in order to assess the practical use of MgAl@WH biochar as an efficient adsorbent. To get rid of contaminants, the real samples were first filtered using a 0.45 mm cellulose membrane. Subsequently, standard mordant brown dye solutions (50 ppm) were added to the resultant real water samples. All batch adsorption tests were run in triplicate, and the findings were given as mean \pm deviation.

3. Results and discussion

3.1. Characterizations

The surface characteristics of the prepared adsorbents (MgAl@WH biochar, MgAl LDH, and WH) were observed by different analytical methods (FTIR, XRD, SEM, TEM, and XPS). The surface functional groups of MgAl@WH biochar, and WH were investigated by FTIR analysis. The FTIR results (Fig. 1A) implied that WH and MgAl@WH had a broad peak at 3374 cm^{-1} were mainly attributed to the O–H stretching vibrations and interlayer water molecules. The shoulders observed at (2849–2918 cm^{-1}) due to C–H stretching vibrations of alkane groups.^{21,25,31} After MgAl LDHs modifications, band intensities of carbonyl C=O (1634 cm^{-1}) groups and aliphatic (C–O–C) (1035 cm^{-1}) decreased.^{21,32,33} Meanwhile, the intensities of the –OH (1362 cm^{-1}) and C=C (1560 cm^{-1}) were strengthened in the FTIR spectra of MgAl@WH biochar. Moreover, MgAl@WH exhibited a well-defined peak at 1362 cm^{-1} related to the presence of Cl^- anions in the LDH structure.^{21,32,33} Additionally, new bands observed within 450–750 cm^{-1} including 443.0, 546.0, 610.0, and 546.0 cm^{-1} could be attributed to the lattice

vibrations of O–Mg(Al)–O, Mg(Al)–OH, and Mg(Al)–O in the layers that can facilitate mordant brown anionic dye adsorption.^{21,32,33} These results confirmed the successful production of MgAl@WH biochar.

The XRD patterns of the prepared MgAl@WH biochar were measured from $2\theta = 5\text{--}80^\circ$ (Fig. 1B). MgAl@WH biochar displayed well-defined diffraction peaks of the LDH structure at 2θ 11.1°, 23.2°, 34.8°, 38.8°, 46.4°, 60.8°, 61.9° which correspond to the (003), (006), (012), (015), (018), (110), and (113) crystal planes of a layered hydrotalcite-like material, respectively, together with diffraction peaks at 65.8° corresponding to the (1, 3, 10) crystal plane.^{21,32–36} The high crystallinity of the (003), (012), and (110) diffraction peaks implies that the prepared MgAl@WH had an analogue interlayer structure. For LDHs, the hydroxide layer's basal spacing can be determined by the value of the (003) reflection using Bragg's law.^{35,37,38} According to Fig. 1B, the interlayer spacing (d_{003}) of MgAl-LDHs was 0.790 nm, indicating a typical layered structure intercalated with chlorides with high crystallinity.³⁵ On the other hand, the hydrothermal preparation of MgAl@WH biochar at high temperature (150 °C, 24 h) facilitates the conversion of some $\text{Al}(\text{OH})_3$ into boehmite ($\gamma\text{-AlOOH}$); therefore, some additional weak peaks at 2θ values of 14.5°, 28.2°, and 48.8°, corresponding to the (020), (120), and (131) crystal planes of boehmite ($\gamma\text{-AlOOH}$), respectively, were observed as shown in Fig. 1B.²¹ The results proved that MgAl LDHs was successfully grafted into the matrix of biochar.

The surface morphology of WH, MgAl LDHs, and MgAl@WH adsorbents was characterized by SEM, as displayed in Fig. 2. As depicted in Fig. 2A–F, the particles of the dried WH are in the form of fibrous rods with very rough and irregular surfaces. While MgAl LDHs-Cl has a uniform particle size with a circular nanoplate shape.⁴ By contrast, the surfaces of the synthesized hydrochar composite were relatively smooth; they were covered with new smooth LDH nanosheets homogenously but with fewer pores and a blocky structure.^{28,32,39} Therefore, the SEM

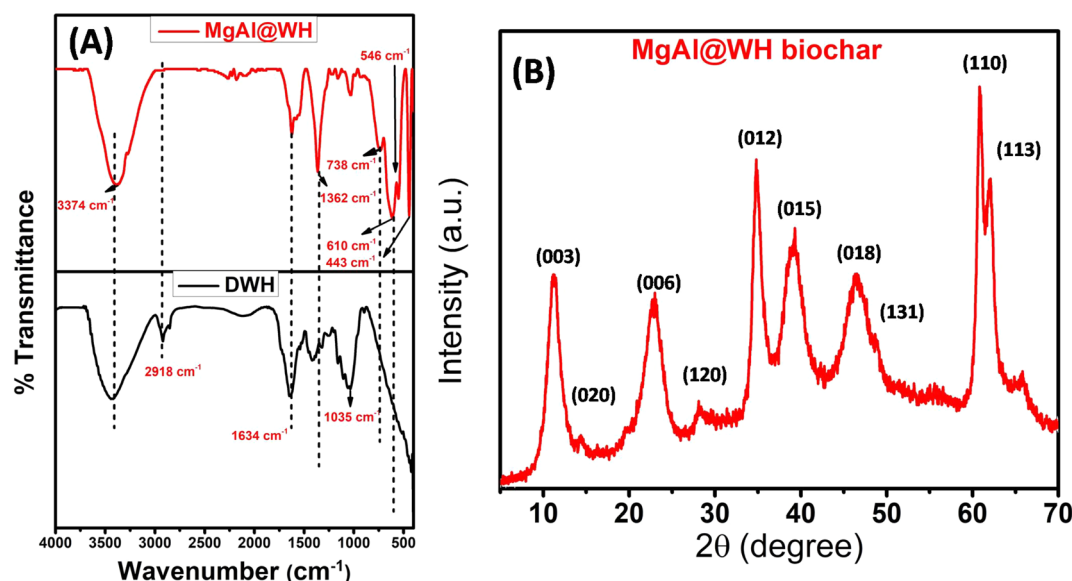


Fig. 1 (A) Fourier transform infrared spectra of WH, and MgAl@WH biochar. (B) XRD patterns of MgAl@WH biochar.



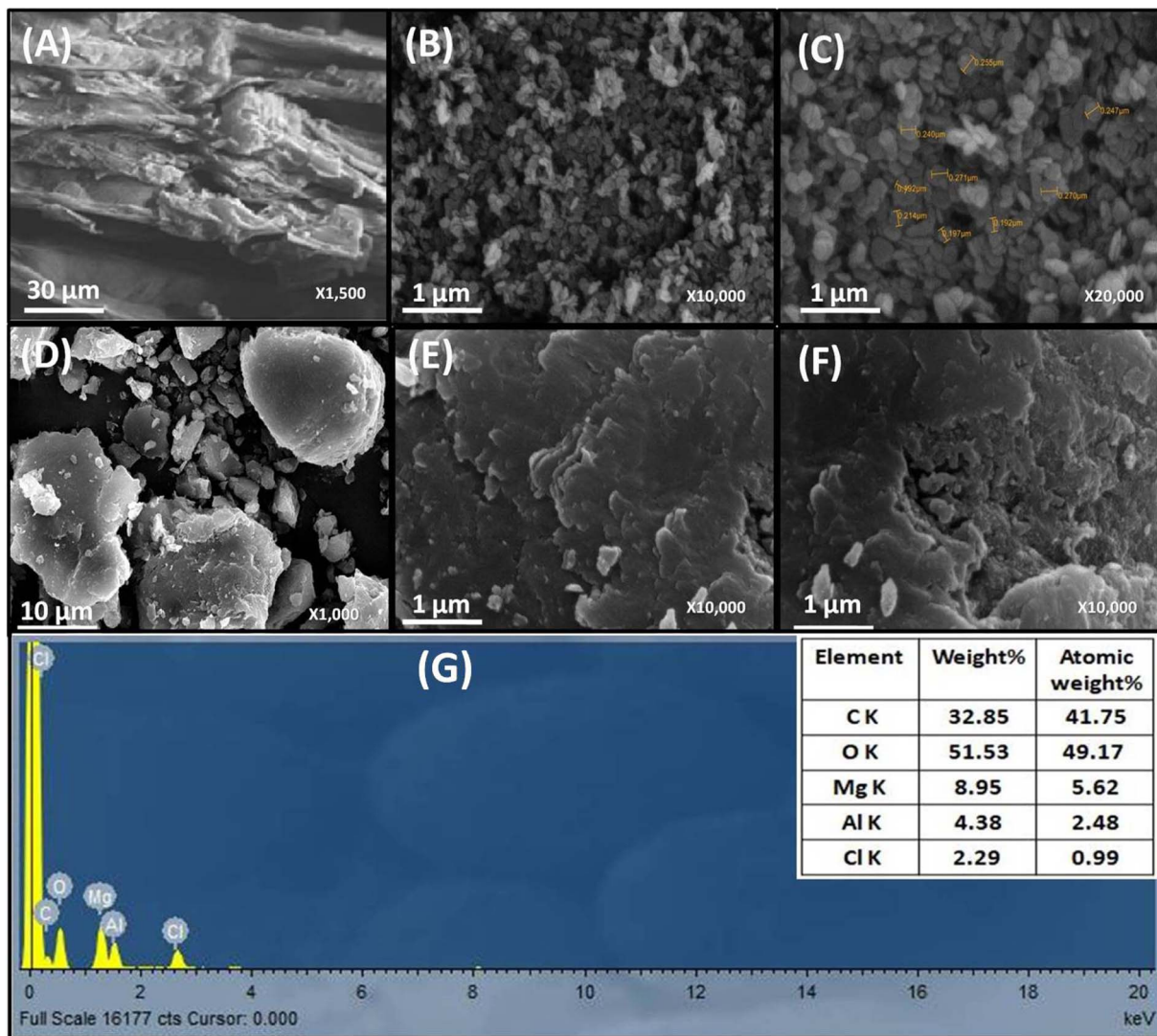


Fig. 2 SEM images of WH (A), MgAl LDH (B and C) and MgAl@WH biochar (D–F). EDX spectrum of MgAl@WH biochar (G).

images demonstrate the successful loading of MgAl onto the surface of WH hydrochar. The EDX analysis showed that MgAl@WH biochar was mainly composed of C (32.85 wt%), O (51.53 wt%), Al (4.38 wt%), Mg (8.95 wt%), and Cl (2.29 wt%) elements, indicating that Mg and Al were loaded chemically on WH biochar as shown in Fig. 2G. Furthermore, as depicted in Fig. 3, EDX was also used to map the Mg, Al, O, Cl, and C distributions in the composite, which provided a visualization of a uniform distribution of Cl, Mg, and Al atoms across the biochar surface. These results confirmed the successful formation of MgAl DLHs all over the biochar with a homogeneous distribution.

The chemical state of the surface elements was detected using XPS analysis. The MgAl LDHs modified water hyacinth hydrochar XPS survey spectra in Fig. 4A demonstrated that the surface elements, including C, O, Mg, Al, and Cl, were present. The high resolution C 1s spectra of MgAl@WH (Fig. 4B) exhibited three peaks at 288.88, 286.38 and 284.98 eV, which might be related to the O–C=O, C–O, and C–C, respectively.^{40,41}

Fig. 4C revealed that three peaks at 529.58, 531.58, and 532.18 eV observed in the O 1s spectrum, and these peaks could be attributed to H₂O physically adsorbed/Al₂O₃, O–M, and OH bonds, respectively.^{42,43} The grafting of the MgAl LDHs onto WH hydrochar was also indicated by the Mg 1s (Fig. 4D) and Al 2p (Fig. 4E). The Mg 1s spectrum could be deconvoluted into two peaks at 1304.0 and 1305.0 eV that could be related to MgO and Mg(OH)₃, respectively.⁴² Additionally, the Al 2p spectra of MgAl@WH exhibited two peaks at 74.33 and 75.1 eV.^{43,44} These peaks could be attributed to Al(OH)₃ and Al₂O₃, respectively, which contributed from the LDH structure.^{43,44} These results were consistent with FTIR, EDX, and XRD and confirmed the successful grafting of MgAl LDHs into WH biochar matrix *via* the hydrothermal method.

3.2. Dye adsorption studies

3.2.1. Influence of solution pH. The solution pH is a crucial factor controlling the dye adsorption process since it has the potential to impact the ionization degree of the adsorbate and



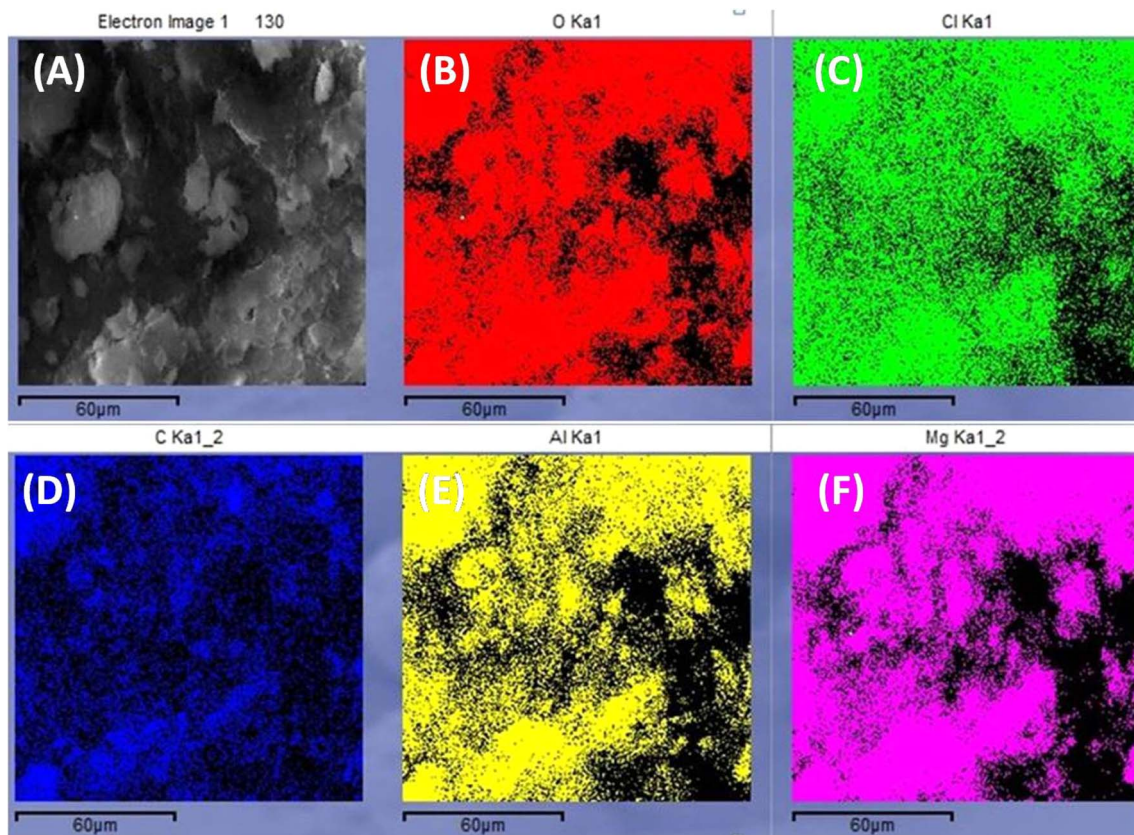


Fig. 3 SEM image of MgAl@WH biochar (A). EDX map of O Ka1 (B), Cl Ka1 (C), C Ka1 (D), Al Ka1 (E), and Mg Ka1 (F) corresponding to A.

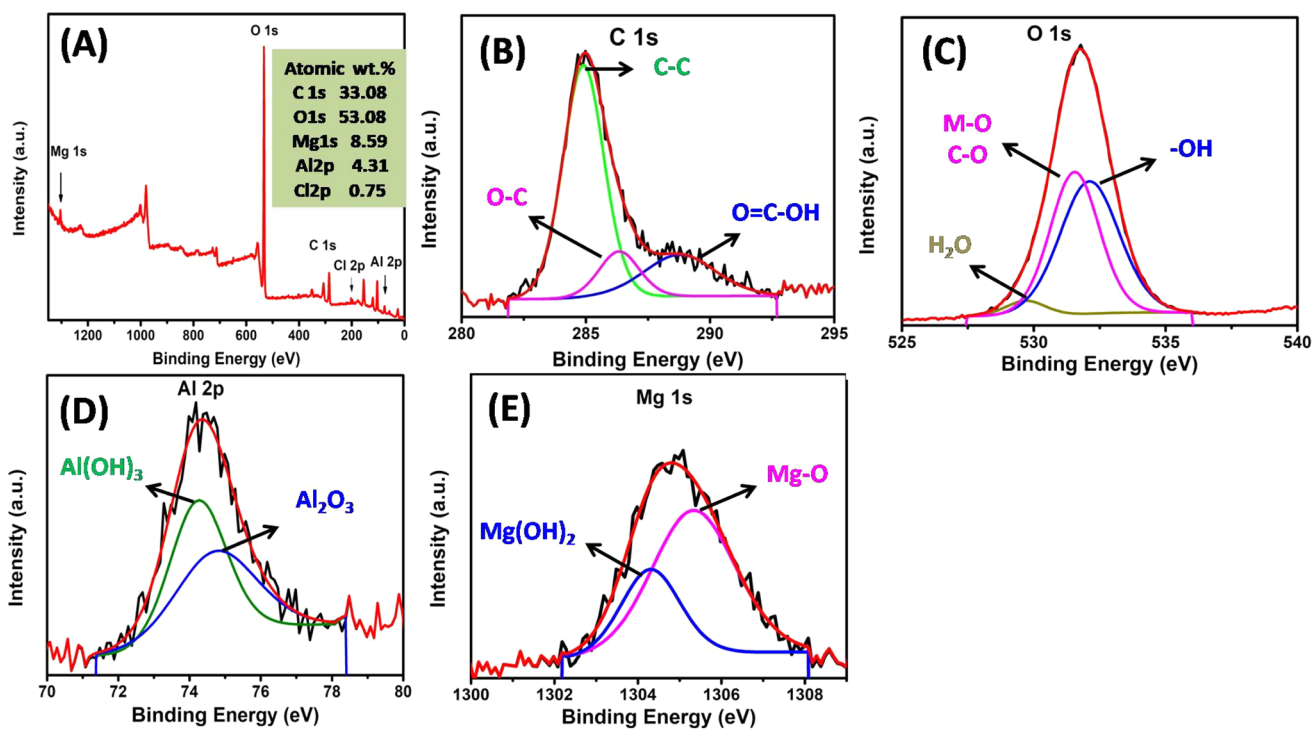


Fig. 4 XPS spectra of MgAl@WH hydrochar (A); high resolution XPS spectra of (B) C 1s, (C) O 1s, (D) Al 2p, (E) Mg 1s.



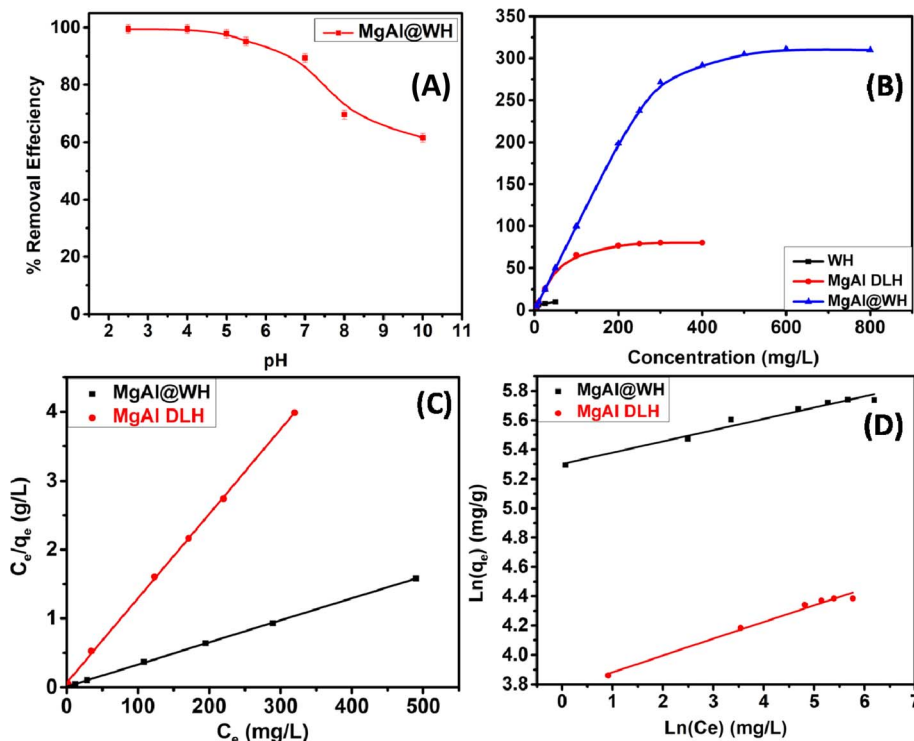


Fig. 5 The adsorption efficiency of MgAl@WH hydrochar as a function of (A) pH; (B) concentration; (C) Langmuir isotherm model and (D) Freundlich isotherm model.

the adsorbent's surface charge. Batch adsorption experiments were conducted to study the impact of various pH values (2.0 to 10.0) on the removal efficiency of mordant brown dye by MgAl@WH biochar, as depicted in Fig. 5A. The results revealed that the maximum adsorption of mordant brown dye (100.0%) onto MgAl@WH biochar was achieved within the pH range (2–5), then slightly decreased (99.55% to 95.5%) in the pH range (5.5–7). Afterward, removal efficiency quickly decreased when the pH was above 7.0. This may be explained in terms of the point of zero charge (PZC) of MgAl@WH biochar and the structure of the anionic mordant brown dye (its pK_a).^{4,45,46} The pH PZC of the MgAl@WH biochar was found to be 5.73, as described in the ESI (S2).† This means that the surface of MgAl@WH biochar was positively charged at $pH < pH_{PZC}$ and negatively charged at $pH > pH_{PZC}$. At pH values higher than 5.73, the adsorption efficiency of anionic mordant brown dye by MgAl@WH biochar decreased sharply due to the electric charge mutual repulsion between the deprotonated (negatively charged) functional groups of MgAl@WH biochar and the sulfonate groups of the anionic (mordant brown) dye molecules.^{4,47} On the other hand, when the pH dropped below 5.73, protonation of the oxygen-containing functional groups increased, enhancing their ability to bind anionic mordant brown dye molecules.^{4,47} These results confirmed that the grafted MgAl LDs on the surface of WH biochar, *via* the hydrothermal method, were the main dye adsorption binding site. As a result, the optimum pH was stated to be roughly 5.5.

3.2.2. Influence of initial concentration. The initial concentration impact on removing mordant brown dye using

MgAl@WH, WH, and MgAl LDHs was conducted using various initial dye concentrations from 1.0 to 800.0 ppm at ambient temperature and pH 5.5. As depicted in Fig. 5B, MgAl@WH biochar exhibited 100% removal for 1–150 ppm mordant brown dye. This might be attributed to the large number of available active sites on MgAl@WH biochar compared to the number of dye molecules. Furthermore, it is clear that as the initial concentration increased, the equilibrium adsorption capacities increased from 1.0 to 10.0 $mg\ g^{-1}$ (for dried water hyacinth (WH)), from 1 to 80.2 $mg\ g^{-1}$ (for MgAl LDHs), and from 1.0 to 311.0 $mg\ g^{-1}$ (for MgAl@WH biochar). Consequently, the combination between MgAl LDHs and WH biochar showed a better adsorption capacity compared to MgAl LDHs and dried WH. This was explained by the fact that, with a greater concentration gradient between the liquid and solid phases, an effective driving force forms, helping to overcome the dye molecules' external mass-transfer resistance.^{48,49} These findings clearly showed that MgAl@WH biochar exhibited superior mordant brown dye adsorption, better than dried water hyacinth and pure MgAl LDHs. This is mainly attributed to the grafting of the positively charged MgAl LDHs into the porous hydrochar derived from water hyacinth in one step through the hydrothermal method. Therefore, MgAl@WH biochar could be used as a potential adsorbent for remediation of textile wastewater containing anionic mordant brown dye compared to the remediation of other anionic dyes using MgAl LDHs and/or biochars prepared through different reported methods (Table S1†).

The Langmuir and Freundlich isotherm models, which describe the equilibrium on both homogeneous and

Table 1 Isotherm parameters for the removal of mordant brown by MgAl@WH hydrochar

Dye	Freundlich parameters				Langmuir parameters			
	1/n	K_F	R^2	Q_{exp} (mg g ⁻¹)	$Q_{\text{max fitted}}$ (mg g ⁻¹)	R_L	b (L mg ⁻¹)	R^2
Mordant brown	0.077	200.667	0.966	311.0	312.5	0.005	0.265	0.999

heterogeneous surfaces, respectively, were applied to elucidate the mordant brown dye adsorption onto MgAl@WH biochar.^{25,50} See ESI (S3)† for further information on the two models and their corresponding equations. For mordant brown adsorption onto MgAl@WH, the results were plotted in Fig. 5. As depicted in Table 1, the correlation coefficient (R^2) value of the Langmuir model is approximately (0.999), and the calculated Q_m (312.5 mg g⁻¹) showed excellent agreement with the experimental q_{max} (311.0 mg g⁻¹). This reveals that the Langmuir model is able to provide a better fit to the equilibrium data than Freundlich model with monolayer adsorption of mordant brown dye on the homogeneous surface of MgAl@WH.⁵¹ Additionally, a favorable adsorption is characterized by R_L value between 0 and 1. Moreover, the Freundlich model's parameter n (12.987) is more than 2, referring that MgAl@WH biochar's adsorption strength to mordant brown anionic dye is comparatively strong.^{25,52}

3.2.3. Kinetic studies. A kinetic study, which describes the rate of mordant brown dye uptake over MgAl@WH biochar at equilibrium time, is one of the most crucial methods used to evaluate adsorption performance. Fig. 6A shows the amount of

mordant brown dye adsorbed (q_t), calculated using eqn (1), over MgAl@WH biochar with the change of time at the initial concentration of 500 ppm and pH 5.5. It was observed that the amount of mordant brown dye adsorbed increased as the agitation time increased. Even with a contact time of five minutes, the extent of adsorption already exceeded 50.0% of the maximum value, and then the rate of adsorption gradually decreased until equilibrium. It was observed that equilibrium was approximately achieved within 120.0 min. In the first five minutes, the interaction between dye molecules and MgAl@WH biochar was easier because there were more adsorption sites available and uncovered surface area on MgAl@WH biochar, as well as a higher driving force.^{25,53} As the adsorption time proceeded further, the adsorption rate gradually decreased until all the MgAl@WH biochar adsorption sites seemed to have been saturated and equilibrium had been reached.⁵⁴ Therefore, MgAl@WH biochar prepared in this study *via* hydrothermal method can be utilized as an efficient adsorbent for the removal of textile organic dyes from wastewater.

Moreover, the pseudo-first-order (PFO) and the pseudo-second-order (PSO) kinetic models were utilized to examine

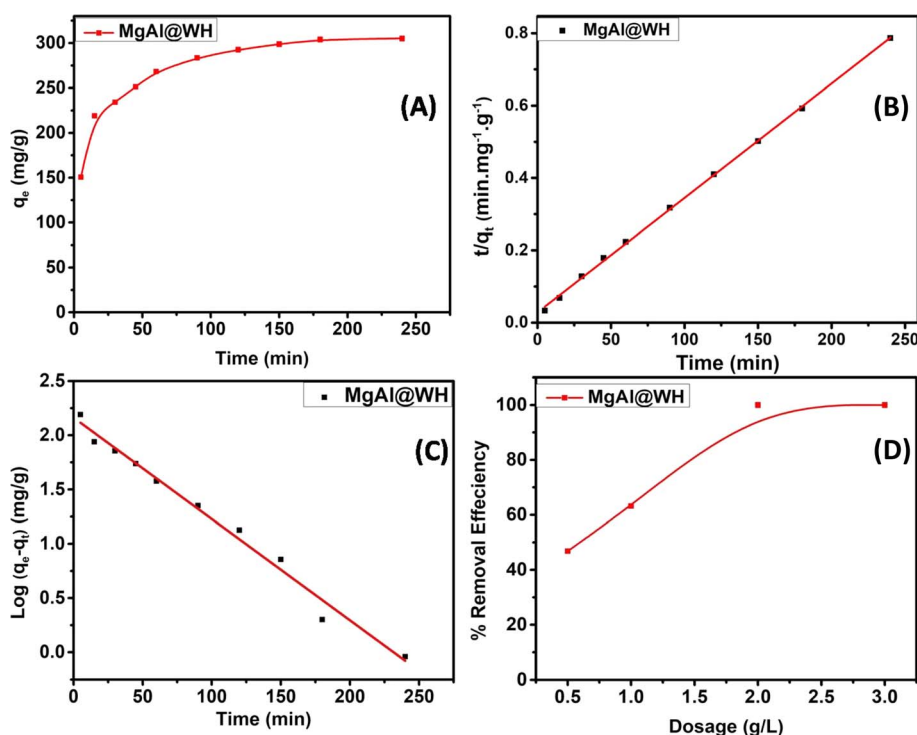


Fig. 6 (A) The adsorption capacity of MgAl@WH hydrochar as a function of contact time; (B) PSO kinetic model; (C) PFO kinetic model; (D) the adsorption efficiency of MgAl@WH hydrochar as a function of adsorbent dosage.



Table 2 Parameters of PSO and PFO models for the adsorption of mordant brown anionic dye onto MgAl@WH biochar

Dye	$q_{e \text{ exp}} (\text{mg g}^{-1})$	PFO parameters			PSO parameters		
		R^2	$q_{e \text{ cal}} (\text{mg g}^{-1})$	$K_1 (\text{min}^{-1})$	R^2	$q_{e \text{ cal}} (\text{mg g}^{-1})$	$K_2 (\text{g mol}^{-1} \text{min}^{-1})$
Mordant brown	306.0	0.984	8.695	0.022	0.999	316.455	0.0004

the kinetic adsorption behaviour of MgAl@WH (Fig. 6). See ESI (S4)† for further information on the two models and their corresponding equations. As presented in Table 2, the correlation coefficient (R^2) of PSO model ($R^2 = 0.999$) is greater than that of PFO.²⁵ Furthermore, the calculated q_e obtained from the PSO is closer to the experimental result. The fitting results demonstrated that the adsorption of mordant brown dye by MgAl@WH biochar was dominated by a pseudo-second-order model through the sharing or exchanging of electrons between mordant brown dye and MgAl@WH biochar.^{25,55}

3.2.4. Impact of temperature and adsorbent dosage. The relationship between temperature and mordant brown dye adsorption onto MgAl@WH was illustrated in Fig. S1.† As presented in Fig. S1,† The highest sorption capacities for the removal of mordant brown dye onto MgAl@WH increased from 311.0 to 401.0 mg g^{-1} when the temperature was elevated from 298 K to

323 K. Since dye molecules' kinetic energy increases with increasing temperature. Additionally, the results demonstrated that the adsorption process of mordant brown is endothermic.⁵⁶ Fig. 6D described the effect of MgAl@WH dosage on the removal of the pungent brown dye. It is evident that by increasing the dosage of MgAl@WH from 0.5 to 2.0 g L^{-1} at pH 5.5 and 500 ppm of the pungent brown dye, the extracted percentage (% E) of the pungent brown dye using MgAl@WH increased from 46.84% to 100.0%. This can be explained by the increased surface area of the sorbent and the availability of more adsorption sites. In contrast, it was observed that as the dose of adsorbent increased, the number of mg of pungent brown dye adsorbed per gram of adsorbent decreased. This may be due to particle accumulation, which reduces the overall surface area of the adsorbent area.^{41,56,57}

3.2.5. Mechanism of adsorption. To further elucidate the possible mordant brown 15 dye adsorption mechanisms of

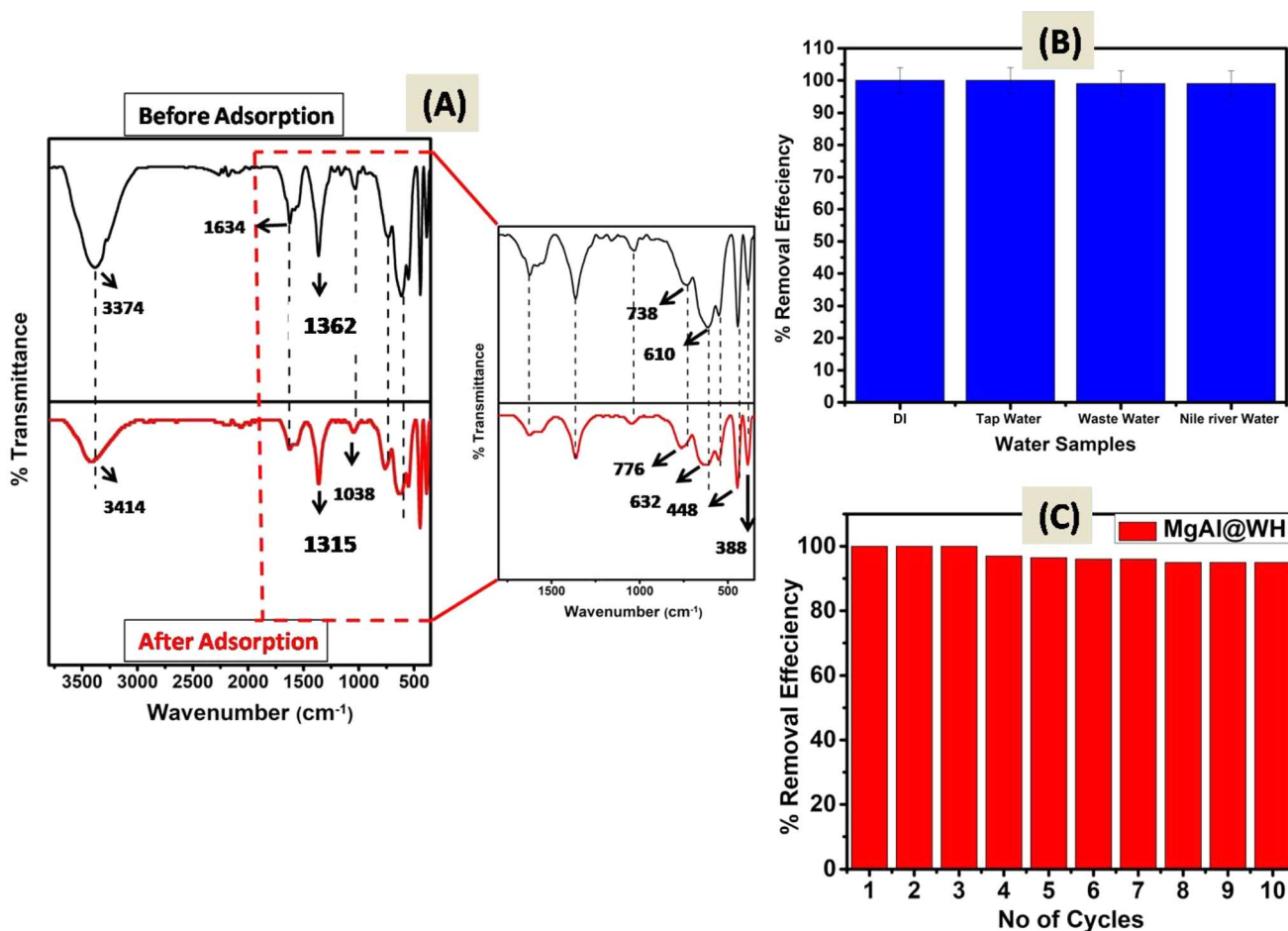
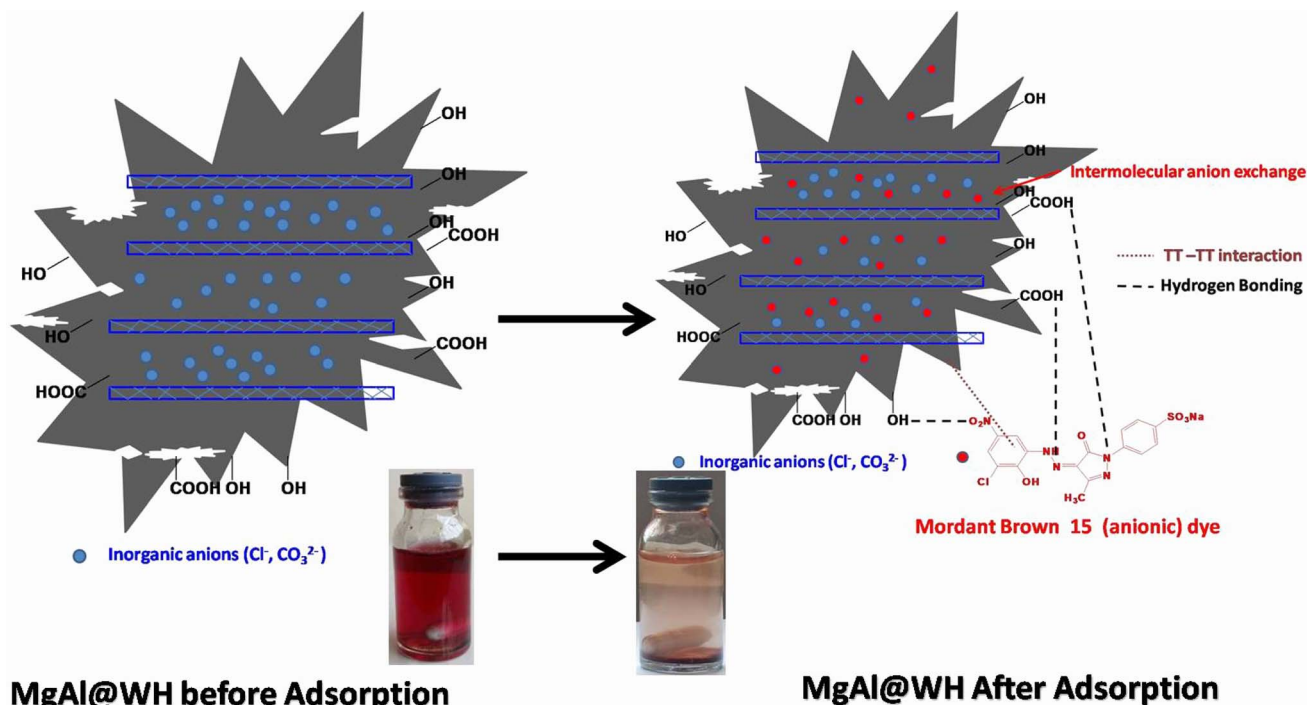


Fig. 7 (A) FTIR spectra of MgAl@WH before and after mordant brown dye adsorption; (B) real water samples analysis and (C) reusability of MgAl@WH adsorbent.





Scheme 2 Possible mechanisms for mordant brown 15 dye adsorption onto MgAl@WH biochar.

MgAl@WH biochar, the FTIR spectra of MgAl@WH biochar before and after mordant brown dye adsorption are described in Fig. 7A. As depicted in Fig. 7A, the intensity of peaks at 738 and 610 cm^{-1} in MgAl@WH, which belong to vibrations of Mg(Al)-OH and Mg(Al)-O, respectively, obviously reduced and shifted to 776 and 632 cm^{-1} after adsorption, providing a proof for the adsorption of mordant brown dye on MgAl@WH biochar.^{5,58} Furthermore, the infrared spectra (Fig. 7A) demonstrated a considerable drop in the intensity of the absorption band at 1362 cm^{-1} , which corresponds to the existence of Cl^- anions as the intercalated anion in the LDH structure after dye adsorption.^{5,21} These findings suggested that during the adsorption processes, anion exchange, or intercalation, occurred between anionic dye molecules and interlayer chloride or carbonate. Furthermore, upon dye adsorption, the peak of MgAl@WH related to OH stretching vibrations (3374 cm^{-1}) was reduced and shifted to 3414 cm^{-1} , suggesting the formation of a hydrogen bonding interaction between the OH of the MgAl@WH biochar surface and the N or O atom of the mordant brown dye molecules.⁵⁸ These results revealed that adsorption *via* hydrogen bonding and interlayer anion exchange are the primary factors in a successful adsorption process, as shown in Scheme 2.

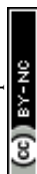
3.2.6. Reusability. One of the most important properties of an adsorbent is its capacity for reuse, as this influences both its long-term and cost-effectiveness in industrial applications. As mentioned in the experimental section, 0.01 M NaOH was used as a desorbing agent (eluent). The regeneration and reusability of the MgAl@WH adsorbent over ten cycles were described in Fig. 7B. The results revealed that the adsorption efficiency was roughly 98.0% after ten cycles. Additionally, there is no

significant change in the FTIR spectrum of MgAl@WH after 10 cycles indicating that MgAl LDHs is not leached from the WH biochar matrix as shown in Fig. S2.† These findings provide valuable insights for the development of biochar-based adsorbent with high stability, efficiency, low cost effectiveness for solving dye pollution.

3.2.7. Real water samples. To evaluate the efficiency and practical applicability of MgAl@WH as an economical and efficient adsorbent, 50 mg L^{-1} of mordant brown was removed from real water samples, such as tap water, Nile River water, and domestic wastewater. As depicted in Fig. 7C, the results revealed that the removal efficiency remained higher than 99.0%. However, river water and wastewater both contain a variety of pollutants and minerals. All batch adsorption tests were run in triplicate with RSD values lower than 4%. These findings supported the viability of using MgAl@WH to remediate wastewater that contains anionic dyes.

4. Conclusions

In this study, the modified water hyacinth biochar with MgAl LDHs was synthesized *via* a simple hydrothermal method. The successful grafting of MgAl LDHs onto the biochar matrix was verified independently by FTIR, XRD, EDX, SEM, and XPS. The adsorption of mordant brown (anionic) dye on MgAl@WH hydrochar was described well using a Langmuir model ($R^2 = 0.999$) and a pseudo-second-order kinetic model ($R^2 = 0.999$), and the maximum adsorption capacity recorded was 311.0 mg g^{-1} . Hydrogen bonding and interlayer anion exchange play a role in the surface adsorption of mordant brown dye. The adsorption and desorption experiments displayed that the



adsorption efficiency was roughly 98.0% after ten cycles. In summary, the findings presented in this research suggest that MgAl@WH exhibits great promise as an adsorbent for the removal of anionic dyes from wastewater.

Author contributions

All authors contributed to the study conception and design. Fathi S. Awad and Saadia M. Waly conceived the project, designed the experiments, analyzed the data, and drafted the manuscript. Ahmad M. El-Wakil analyzed the data, reviewed and edited the manuscript. Weam M. Abou El-Maaty contributed to the characterization of the samples. All the authors discussed the results and commented on the manuscript.

Conflicts of interest

There are no conflicts to declare.

References

- 1 M. F. Akhtar, M. Ashraf, A. Javeed, A. A. Anjum, A. Sharif, A. Saleem, B. Akhtar, A. M. Khan and I. Altaf, *Bull. Environ. Contam. Toxicol.*, 2016, **96**, 502–507.
- 2 M. Al-Ghouti, M. Khraisheh, S. Allen and M. Ahmad, *J. Environ. Manage.*, 2003, **69**, 229–238.
- 3 V. Gupta, *J. Environ. Manage.*, 2009, **90**, 2313–2342.
- 4 L. Ai, C. Zhang and L. Meng, *J. Chem. Eng. Data*, 2011, **56**, 4217–4225.
- 5 S. Lei, S. Wang, B. Gao, Y. Zhan, Q. Zhao, S. Jin, G. Song, X. Lyu, Y. Zhang and Y. Tang, *J. Colloid Interface Sci.*, 2020, **577**, 181–190.
- 6 K. Dutta, S. Mukhopadhyay, S. Bhattacharjee and B. Chaudhuri, *J. Hazard. Mater.*, 2001, **84**, 57–71.
- 7 M. Kornaros and G. Lyberatos, *J. Hazard. Mater.*, 2006, **136**, 95–102.
- 8 S. Mozia, A. W. Morawski, M. Toyoda and T. Tsumura, *Desalination*, 2010, **250**, 666–672.
- 9 M. Buonomenna, A. Gordano, G. Golemme and E. Drioli, *React. Funct. Polym.*, 2009, **69**, 259–263.
- 10 J.-W. Lee, S.-P. Choi, R. Thiruvengatachari, W.-G. Shim and H. Moon, *Water Res.*, 2006, **40**, 435–444.
- 11 H. Selcuk, *Dyes Pigm.*, 2005, **64**, 217–222.
- 12 M. Muruganandham and M. Swaminathan, *J. Hazard. Mater.*, 2006, **135**, 78–86.
- 13 B. Zhao, Y. Zhao, P. Liu, Y.-L. Men and Y.-X. Pan, *Green Chem. Eng.*, 2023, **4**, 88–98.
- 14 S.-T. Yang, S. Chen, Y. Chang, A. Cao, Y. Liu and H. Wang, *J. Colloid Interface Sci.*, 2011, **359**, 24–29.
- 15 M. Ghaedi, F. Karimi, B. Barazesh, R. Sahraei and A. Daneshfar, *J. Ind. Eng. Chem.*, 2013, **19**, 756–763.
- 16 M. Wawrzekiewicz, E. Polska-Adach and Z. Hubicki, *Sep. Sci. Technol.*, 2020, **55**, 2122–2136.
- 17 K.-W. Jung, M.-J. Hwang, T.-U. Jeong and K.-H. Ahn, *Bioresour. Technol.*, 2015, **191**, 342–345.
- 18 Y. Chen, B. Wang, J. Xin, P. Sun and D. Wu, *Ecotoxicol. Environ. Saf.*, 2018, **164**, 440–447.
- 19 K. N. Palansooriya, Y. Yang, Y. F. Tsang, B. Sarkar, D. Hou, X. Cao, E. Meers, J. Rinklebe, K.-H. Kim and Y. S. Ok, *Crit. Rev. Environ. Sci. Technol.*, 2020, **50**, 549–611.
- 20 Y. Deng, M. Li, Z. Zhang, Q. Liu, K. Jiang, J. Tian, Y. Zhang and F. Ni, *J. Environ. Chem. Eng.*, 2021, **9**, 105079.
- 21 K.-W. Jung, S. Y. Lee, J.-W. Choi, M.-J. Hwang and W. G. Shim, *Chem. Eng. J.*, 2021, **420**, 129775.
- 22 V.-T. Nguyen, T.-B. Nguyen, C.-W. Chen, C.-M. Hung, J.-H. Chang and C.-D. Dong, *Bioresour. Technol.*, 2019, **284**, 197–203.
- 23 Y. Li, N. Tsend, T. Li, H. Liu, R. Yang, X. Gai, H. Wang and S. Shan, *Bioresour. Technol.*, 2019, **273**, 136–143.
- 24 Y. Li, A. Meas, S. Shan, R. Yang, X. Gai, H. Wang and N. Tsend, *Bioresour. Technol.*, 2018, **261**, 257–264.
- 25 J.-C. Zheng, H.-M. Feng, M. H.-W. Lam, P. K.-S. Lam, Y.-W. Ding and H.-Q. Yu, *J. Hazard. Mater.*, 2009, **171**, 780–785.
- 26 X. Ji, Y. Liu, Z. Gao, H. Lin, X. Xu, Y. Zhang, K. Zhu, Y. Zhang, H. Sun and J. Duan, *Sep. Purif. Technol.*, 2024, **330**, 125235.
- 27 F. Zhang, X. Wang, J. Xionghui and L. Ma, *Environ. Pollut.*, 2016, **216**, 575–583.
- 28 Q. Yin, H. Ren, R. Wang and Z. Zhao, *Sci. Total Environ.*, 2018, **631**, 895–903.
- 29 S. V. Novais, M. D. O. Zenero, J. Tronto, R. F. Conz and C. E. P. Cerri, *J. Environ. Manage.*, 2018, **214**, 36–44.
- 30 F. S. Awad, K. M. AbouZeid, W. M. A. El-Maaty, A. M. El-Wakil and M. S. El-Shall, *ACS Appl. Mater. Interfaces*, 2017, **9**, 34230–34242.
- 31 P. Kumar and M. Chauhan, *J. Environ. Chem. Eng.*, 2019, **7**, 103218.
- 32 Y. Peng, Y. Sun, A. Hanif, J. Shang, Z. Shen, D. Hou, Y. Zhou, Q. Chen, Y. S. Ok and D. C. Tsang, *J. Cleaner Prod.*, 2021, **289**, 125142.
- 33 R. Li, J. J. Wang, B. Zhou, M. K. Awasthi, A. Ali, Z. Zhang, L. A. Gaston, A. H. Lahori and A. Mahar, *Sci. Total Environ.*, 2016, **559**, 121–129.
- 34 F. Zhang, M. Sun, S. Xu, L. Zhao and B. Zhang, *Chem. Eng. J.*, 2008, **141**, 362–367.
- 35 Y. Cao, D. Zheng, S. Dong, F. Zhang, J. Lin, C. Wang and C. Lin, *J. Electrochem. Soc.*, 2019, **166**, C3106.
- 36 M. Zheludkevich, S. Poznyak, L. Rodrigues, D. Raps, T. Hack, L. Dick, T. Nunes and M. Ferreira, *Corros. Sci.*, 2010, **52**, 602–611.
- 37 S. Poznyak, J. Tedim, L. Rodrigues, A. Salak, M. Zheludkevich, L. Dick and M. Ferreira, *ACS Appl. Mater. Interfaces*, 2009, **1**, 2353–2362.
- 38 Z. Yang, H. Fischer, J. Cerezo, J. Mol and R. Polder, *Mater. Corros.*, 2016, **67**, 721–738.
- 39 Q. Yin, R. Wang and Z. Zhao, *J. Cleaner Prod.*, 2018, **176**, 230–240.
- 40 S. M. Waly, A. M. El-Wakil, W. M. Abou El-Maaty and F. S. Awad, *J. Saudi Chem. Soc.*, 2021, **25**, 101296.
- 41 A. M. El-Wakil, S. M. Waly, W. M. Abou El-Maaty, M. M. Waly, M. Yilmaz and F. S. Awad, *ACS Omega*, 2022, **7**, 6058–6069.
- 42 F. Zhang, C.-L. Zhang, L. Song, R.-C. Zeng, L.-Y. Cui and H.-Z. Cui, *Acta Metall. Sin.*, 2015, **28**, 1373–1381.



- 43 G. Zheng, C. Wu, J. Wang, S. Mo, Z. Zou, B. Zhou and F. Long, *Nanoscale Res. Lett.*, 2019, **14**, 1–12.
- 44 X. Guo, S. Xu, L. Zhao, W. Lu, F. Zhang, D. G. Evans and X. Duan, *Langmuir*, 2009, **25**, 9894–9897.
- 45 L. Yang, Z. Shahrivari, P. K. Liu, M. Sahimi and T. T. Tsotsis, *Ind. Eng. Chem. Res.*, 2005, **44**, 6804–6815.
- 46 D. P. Das, J. Das and K. Parida, *J. Colloid Interface Sci.*, 2003, **261**, 213–220.
- 47 A. Chakraborty and H. Acharya, *Colloid Interface Sci. Commun.*, 2018, **24**, 35–39.
- 48 X. Qi, Q. Zeng, X. Tong, T. Su, L. Xie, K. Yuan, J. Xu and J. Shen, *J. Hazard. Mater.*, 2021, **402**, 123359.
- 49 F. S. Awad, A. M. Bakry, A. A. Ibrahim, A. Lin and M. S. El-Shall, *Ind. Eng. Chem. Res.*, 2021, **60**, 12675–12688.
- 50 A. M. Bakry, W. M. Alamier, R. S. Salama, M. S. El-Shall and F. S. Awad, *Surf. Interfaces*, 2022, **31**, 102006.
- 51 B. Ren, Y. Xu, L. Zhang and Z. Liu, *J. Taiwan Inst. Chem. Eng.*, 2018, **88**, 114–120.
- 52 D. Borah, S. Satokawa, S. Kato and T. Kojima, *J. Colloid Interface Sci.*, 2008, **319**, 53–62.
- 53 M. Alkan, M. Doğan, Y. Turhan, Ö. Demirbaş and P. Turan, *Chem. Eng. J.*, 2008, **139**, 213–223.
- 54 R. S. Salama, E.-S. M. El-Sayed, S. M. El-Bahy and F. S. Awad, *Colloids Surf., A*, 2021, **626**, 127089.
- 55 Y.-S. Ho and G. McKay, *Chem. Eng. J.*, 1998, **70**, 115–124.
- 56 N. M. Ghazy, E. A. Ghaith, Y. Abou El-Reash, R. R. Zaky, W. M. Abou El-Maaty and F. S. Awad, *RSC Adv.*, 2022, **12**, 35587–35597.
- 57 F. S. Awad, K. M. AbouZied, W. M. Abou El-Maaty, A. M. El-Wakil and M. S. El-Shall, *Arabian J. Chem.*, 2020, **13**, 2659–2670.
- 58 Z. Jin, X. Wang, Y. Sun, Y. Ai and X. Wang, *Environ. Sci. Technol.*, 2015, **49**, 9168–9175.

